A 2D rhomboidal system of manganese(II) [Mn(3-MeC6H4COO)2(H2O)2]n with spin canting: rationalization of the magnetic exchange†

Beltzane Garcia-Cirera, [a] Ramon Costa, [a,b] Ibério de P. R. Moreira, [*b,c]
Mercè Font-Bardia [d,e] and Montserrat Corbella [*a,f]

a Departament de Química Inorgànica i Orgànica, Secció Química Inorgànica, Universitat de Barcelona, Martí i Franquès 1-11, 08028-Barcelona, Spain.
b Institut de Química Teòrica i Computacional (IQTCUB), Universitat de Barcelona, Martí i Franquès 1-11, 08028-Barcelona, Spain.
c Departament de Ciència de Materials i Química Física, Secció Química Física, Universitat de Barcelona, Martí i Franquès 1-11, 08028-Barcelona, Spain
d Unitat de Difracció de RX, Centres Científics i Tecnològics de la Universitat de Barcelona (CCiTUB), Universitat de Barcelona, Solé i Sabarís 1-3, 08028-Barcelona, Spain
e Departament de Mineralogia, Petrologia i Geologia Aplicada, Facultat de Ciències de la Terra, Universitat de Barcelona, Martí i Franquès s/n, 08028-Barcelona, Spain
f Institut de Nanociència i Nanotecnologia (IN2UB), Universitat de Barcelona, Martí i Franquès 1-11, 08028-Barcelona, Spain

Montserrat Corbella: montse.corbella@ub.edu.
Ibério de P. R. Moreira : i.moreira@ub.edu

ABSTRACT:

The crystal structure of Mn(II) carboxylate with 3-methylbenzoate as a bridging ligand [Mn(3-MeC6H4COO)2(H2O)2]n shows a rhomboidal layer, where each pair of neighbor Mn(II) ions are bridged through only one carboxylate group with a syn–anti conformation. The magnetic exchange between neighbor ions is weakly antiferromagnetic (J = −0.52 cm−1, g = 2.04), and at low temperature the system shows spin canting with TB = 3.8 K. Computational studies, based on periodic calculations of the energies of the significant spin states on the magnetic cell and some higher supercells, corroborate the weak AF interaction between the adjacent Mn(II) ions and preclude the negligible effect of frustration caused by very weak interactions between the non-adjacent ions in the magnetic response of the system. The results provide compelling evidence that the observed spin canting is due to the local coordination geometry of the manganese ions leading to two antiferromagnetically coupled subnets with different axial vectors.

INTRODUCTION

Carboxylate ligands are of great interest in coordination chemistry due to their ability to coordinate metal ions leading to systems with a wide range of nuclearity. This rich diversity of structures is related to their coordination mode versatility. A carboxylate bridging ligand could be coordinated in different modes and this fact influences the magnetic exchange between the metallic ions. The simplest coordination mode is a μ1,3 bridge that can be arranged in a syn–syn, syn–anti or anti–anti fashion. It is well known that the magnetic exchange through the carboxylate bridge is weak, however, some differences have been observed, the antiferromagnetic interaction being stronger for the syn–syn coordination mode than for the other conformations.1

Most of the Mn(II) polymeric or extended compounds with carboxylate ligands have two or three bridging ligands that can be a carboxylate or carboxylate and another ligand. In the last few years a wide range of manganese(II) carboxylates with polycarboxylate ligands has been reported.2–10 However, the number of systems where the manganese(II) ions are bridged through only one carboxylate group is rather scarce. To the best of our knowledge, two chains have been reported, one with the carboxylate in a syn–anti conformation,11 and the other with an anti–anti conformation,12 a 3D system13 and three 2D systems where the carboxylate group bridges the Mn (II) ions in a syn–anti conformation.14–17

Despite the weak magnetic interaction expected for Mn(II) systems with only carboxylate bridging ligands, the flexibility and versatility in their coordination mode could provide a way to obtain 1D and 2D magnetically ordered systems. There are several examples of systems with an antiferromagnetic interaction between similar spins that show weak ferromagnetism at low temperature, due to the non-perfect alignment of the antiferromagnetically coupled spins (spin canting).18–21

In this work we report the synthesis, crystal structure and magnetic properties of a new 2D magnetic system with the chemical formula [Mn(3-MeC6H4COO)2(H2O)2]n and a syn–anti conformation of the carboxylate ligand. The analysis of the experimental magnetic data has been carried out by a fitting procedure using the expansion series for a weakly anisotropic quadratic-layer antiferromagnet reported by Lines.22 This methodology provides the value for the exchange coupling constant J between the neighboring Mn(II) ions. One computational approach to obtain the J value theoretically is the division of the layer in equivalent dinuclear Mn(II)–Mn(II) fragments and calculate the magnetic interaction inside one of them. Although this dominant coupling constant alone can be considered the leading interaction on the system, the theoretical analysis of the magnetic properties for a 2D magnetic net is not trivial: this methodology stands only for a local description and ignores the real dimensionality of the system, the interactions between the non-adjacent ions, and the reciprocal influence between the different couplings.23 In addition, for very weak magnetic interactions the fitting of the magnetic data can lead to some uncertainties on the magnitude or even on the sign of the exchange coupling constants when error intervals are of the order of the J value. These facts can be important for bi-dimensional systems and an estimation of the non-neighboring Mn(II) coupling constants can be valuable to interpret

the low temperature magnetic behavior. To overcome these uncertainties we propose to perform a computational study using periodic calculations with hybrid DFT functionals by means of the CRYSTAL code24 to evaluate in a consistent way both the nearest-neighbor and the non-adjacent ions' magnetic coupling constants from the energies of the significant spin states on the magnetic cell and some higher supercells. This methodology has been carried out for Cu(II) and Ni(II) ionic lattices,23,25 and we try to extend its use to the more complex polymeric coordination compounds containing 5 unpaired electrons in each paramagnetic center. This kind of calculation is scarce and can be useful to support the interpretation of the experimental magnetic data or to suggest the need for using alternative approaches.

RESULTS AND DISCUSSION

Description of the crystal structure

The asymmetric unit of compound 1 shows a Mn(II) ion, one carboxylate ligand and one water molecule (Fig. S1 of the ESI†); the octahedral environment of the manganese ion is generated by symmetry. A view of the sheet is depicted in Fig. 1 and Fig. 2 shows the environment of four Mn(II) ions in the crystal structure of compound 1, where the 3-MeC6H4 groups are omitted for a better visualization of the disposition of the Mn(II) ions in the layer. The most relevant interatomic distances and angles are shown in Table 1.

Four carboxylate ligands are placed in the equatorial plane of the octahedron and the axial positions are occupied by water molecules. Each carboxylate ligand bridges two metallic centers in a μ1,3 mode and a syn–anti conformation, generating a wavy sheet with all the Mn(II) ions in the same plane. The layer consists of a repetition of rhombi of four Mn(II) ions with each pair of ions bridged through only one carboxylate ligand. In the rhombus, two water ligands coordinated to the opposite metallic centers point to the inside of the ring.

All the Mn–O distances are very similar; the Mn–Ocarboxylate distances (Mn–O1 and Mn–O2) are slightly shorter (2.172 and 2.175 Å, respectively) than the Mn–Ow distances (2.178 Å). Therefore, the coordination octahedra are slightly elongated in the direction of water ligands. The phenyl ring is almost coplanar to the carboxylate group. The Mn···Mn distances between the adjacent Mn(II) ions (A···B and A···D) are 4.99 Å, while between the opposite ions, the distances are not equivalent: the Mn_B···Mn_D distance (6.89 Å) is shorter than the Mn_A···Mn_C distance (7.23 Å) (Fig. 2). Consequently, two different angles are found between the Mn(II) ions: α(Mn_A–Mn_B–Mn_C) is 87.28° while β(Mn_B–Mn_A–Mn_D) is 92.72°. Hence, we conclude that the structure of this compound could be described, from the crystallographic point of view, as a rhombic layer.

The four Mn(II) ions in the rhombus are in the same plane; the coordination octahedra of the alternated ions are parallel (Mn_B and Mn_D, Mn_A and Mn_C), while the coordination octahedra of the adjacent Mn(II) ions are tilted, the angle between the elongation axis being τ(Ow–Mn···Mn–Ow) = −71.2° (Fig. 3).

The Ow···Ow distance between the water molecules coordinated to the non-adjacent Mn(II) ions is 3.634 Å; due to the syn–anti conformation of the carboxylate bridging ligands, there are hydrogen bonds between the water molecules and the carboxylate ligands (d(O2···Ow) = 2.714 and 2.78 Å) (Fig. S2 of the ESI†).

The separation between the layers is 16 Å and due to the steric hindrance of the methyl group of the carboxylate ligands, shows a staggered disposition, as shown in Fig. S3 of the ESI.†

Magnetic properties

The variable-temperature magnetic susceptibility of 1 was measured under various applied fields of 3000–13.5 G, exhibiting a strong field-dependent magnetic behavior. Under an applied magnetic field of 3000 G the χMT value is 4.44 cm3 mol−1 K at 300 K, which is in good agreement with the spin-only value for one isolated high-spin MnII ion with g = 2.0. Upon cooling, the χMT value decreases to a minimum of 0.7 cm3 mol−1 K at 3.3 K, indicating an antiferromagnetic coupling between the adjacent Mn(II) ions (Fig. 4). A small peak is observed from the χMT vs. T plot below 5 K, when the applied field is small (200 G or lower). An anomalous behaviour is also observed from the χM vs. T plot that shows two maxima (Fig. 4, inset), at 6 K (χM ~ 0.24 cm3 mol−1) and at 3 K (χM ~0.31 cm3 mol−1). The experimental data between 300 and 5 K were fit by using the expansion series of Lines22 for a quadratic-layer of Mn(II) ions (see the Experimental section). The best fit for the χMT (and χM) data was obtained with J = −0.52 (−0.47) cm−1, g = 2.04 (2.0) and R = 1.20 10−4 (1.38 10−4). This value is in the range found for systems with only one carboxylate ligand bridging the Mn(II) ions (~0 to −1.1 cm−1).1,11–14

Below 5 K, the χMT values increase abruptly up to a sharp maximum at 3.5 K and finally decrease again until 2 K. This fact suggests the existence of a weak long-range ferromagnetic order below 4 K. The value of the χMT maximum becomes strongly field-dependent (Fig. 5); this behavior is characteristic of spin canting,26 which was further evidenced in the bifurcated field-cooling (FC) and zero-field-cooling (ZFC) χMT vs. T plot for an applied field of 85 G (Fig. 6). The divergence of the ZFC and FC data below Tc = 3.8 K indicates some irreversibility arising from the formation of an ordered magnetic state. The shape of the isothermal magnetization plot at 2 K (Fig. 7) indicates that this system exhibits metamagnetism, with the antiferromagnetic to ferromagnetic transition near 1000 G. The magnetic hysteresis curve is shown in Fig. S4 (ESI†).

The observed weak ferromagnetism may originate from spin canting: the local spin of the neighbor Mn(II) ions coupled antiferromagnetically is not completely antiparallel but canted to each other, resulting in an uncompensated residual spin on the rhombic unit. The correlation between the residual spins may lead to a long-range ordering as suggested by the χMT curves and ZFC and FC experiments. The observed magnetic order at low temperatures (spin canting) can be explained by the tilting of the coordination octahedral of the neighboring Mn(II) ions as shown in Fig. 3.

AC susceptibility measurements at two frequencies (10 Hz and 900 Hz) gave superimposable graphs, indicating that the system does not show relaxation of the magnetization (Fig. S5, ESI†).

As indicated, there are two compounds reported in the literature with similar topology and only one carboxylate group bridging neighbor Mn(II) ions, [Mn(BTA)2(H2O)2]n (A) (BTA− is 2-(1H-benzotriazol-1-yl)acetate)14 and [Mn(tp)(H2O)2]n (B) (tp2– is terephthalate).16,17 The three compounds (1, A and B) show weak antiferromagnetic behavior, with A being weaker than 1 or B (any maximum on the χM vs. T graph was observed). However, the most significant difference between these compounds is found at low temperatures. Compound 1 shows spin canting while no order was observed

for A. This difference can be attributed to the relative disposition of the distortion axes of the neighboring octahedra on the sheet. The τ(Ow–Mn···Mn–Ow) angle for A is 31.4° while for 1 is 71.2°. Compound B also shows magnetic order at a low temperature.16 Hence, the difference in the carboxylate bridge (steric hindrance and possibility to form hydrogen bonds) is crucial to the disposition of the ligands around the Mn(II) ions and consequently to the presence or absence of spin-canting.

Theoretical analysis

The magnetic properties of compound 1 have been evaluated from a theoretical point of view using band structure calculations, by estimating the coupling interaction between the adjacent and non-adjacent Mn(II) magnetic centers and its possible influence on the low temperature magnetic behavior. The relevant interactions between the metal ions can be represented over the crystallographic unit cell as depicted in Fig. 8.

Calculations have been performed using the experimental crystal structure described in the previous section. Taking advantage of its small size, we have built two different magnetic cells corresponding to the full ferromagnetic (FM) and the full antiferromagnetic (AF) spin configurations (Fig. 9). According to the experimental data, the AF solution should represent the spin distribution of the magnetic ground state of the system and the FM solution should correspond to the highest energy configuration.

The energy gap between these solutions can be related to a given linear combination of the magnetic coupling constants of the magnetic system. In fact, to obtain the three J1, J2 and J3 values for compound 1 we need two additional energy differences, in order to establish and solve a linear system of three independent equations. We have then designed two magnetic supercells corresponding to the unit cell doubled along the b and c crystallographic axes (Fig. 10) which describe two new and independent spin distributions (AF2b and AF2c, respectively) which preserve the periodic congruence.

To extract the magnetic coupling constants from the energy differences between these magnetic solutions a mapping procedure has been applied following previous studies carried out by some of the authors [see for instance ref. 22 and 24 and references therein]. This mapping procedure considers the Ising Hamiltonian (spin Hamiltonian $H = -\Sigma ij(JijSzi \cdot Szj)$ up to the third nearest neighbor) to provide explicit relations for the expectation values of the energy differences.

As we have performed the calculations over different multiples of the crystallographic cell, we have referred to the energies of all the magnetic solutions per Mn ion as depicted in Fig. 11.

The electronic band structure calculations using the magnetic cells mentioned above describe the system as an antiferromagnetic insulator (indirect gap of 4.6 eV at the B3LYP level for all magnetic solutions) with a spin density strongly localized on the Mn(II) centers, corresponding to S = 5/2 spin particles. The most stable magnetic solution corresponds to the AF solution, in agreement with the experimentally observed behavior.

Regarding the magnetic interactions, using a reasonably accurate basis set (BS2 in the Computational details section) with the B3LYP functional to estimate the energy differences between different

magnetic solutions shown in Fig. 9, the calculated values are J1 = −1.200 cm−1, J2 = −0.007 cm−1 and J3 = −0.003 cm−1. The very small values of J2 and J3 indicate that J1 is the dominant magnetic interaction, leading to describe the magnetic system for this compound as a non-frustrated rhomboidal 2D antiferromagnetic structure. A better estimate of the magnitude of J1 can be obtained using the very large all electron basis set (BS1 in the Computational details section) for all atoms: calculations with the B3LYP functional gave J1 = −1.009 cm−1 and with the PBE0 functional the value was J1 = −0.745 cm−1. The smaller value provided by PBE0 is expected due to the larger amount of Fock exchange in this functional (25%) compared to B3LYP (20%) and in line with previously reported calculations.23,25 It is worth mentioning that calculations on the double supercells using the BS1 basis set are unaffordable, so only the J1 value can be obtained at this precision level. To summarize, the electronic structure calculations describe this system as an antiferromagnetic insulator showing a simple 2D rhombic antiferromagnetic structure dominated by the nearest neighbor interaction J1. Hence, the weak ferromagnetic behavior observed below 4 K can be assigned to a canted antiferromagnetic structure induced by the tilting of coordination octahedra.

For comparison, a rough estimation of the main exchange coupling constant has been performed from calculations on the dinuclear fragment [Mn2(RCOO)7(H2O)4]3− where the complete metal coordination spheres are included. The obtained values are −1.53 cm−1 for the B3LYP functional and −1.12 cm−1 for PBE0, which are almost 50% overestimated with respect to the periodic calculations using comparable all electron basis sets.

EXPERIMENTAL

Synthesis of [Mn(3-MeC6H4COO)2(H2O)2]n (1)

To a suspension of 22 mmol (2.5 g) of MnCO3 in 500 mL of water an aqueous suspension of 37 mmol (5 g) of 3-MeC6H4COOH was added. The resulting mixture in a volume of ∼1 L was heated for 24 hours at 80 °C, with constant stirring. Then, the warm suspension was filtered with the aim to remove the excess of MnCO3 and some MnO2 formed during the reaction. The clear solution was concentrated until ∼200 mL and then left undisturbed at room temperature. The pale rose crystalline product was filtered, washed with ether and dried in air. Good crystals suitable for X-ray diffraction were obtained from the mother liquor, after removing the first fraction of 1. Yield 4.3 g (64%). Anal. calcd for MnC16H18O6 (361.25 g mol−1): C, 53.20; H, 5.02. Found: C, 53.4; H, 4.9. IR (KBr, cm−1): 3400 (m), 1597 (m), 1545 (s), 1484 (w), 1432 (m), 1395 (m), 753 (s), 675 (m). The three bands at 1600, ∼1545 and ∼1395 cm−1 can be assigned to the asymmetric (the two former) and symmetric vibrations from the carboxylate group; the gap between these vibrations, $\Delta = \nu a(COO) - \nu s(COO) \sim 200$ cm−1 is indicative of the carboxylate ligands coordinated in a bidentate bridging mode (μ1,3).27

Physical measurements

Analyses of C and H were carried out by the "Servei de Microanàlisi" of the "Institut de Quimica Avançada de Catalunya, IQAC, Consell Superior d'Investigacions Científiques (CSIC)". Infrared spectra were recorded on KBr pellets in the range of 4000–400 cm−1, with a Termo Nicolet Avatar 330 FT-IR spectrometer. All magnetic measurements were carried out on a Quantum Design MPMS XL5 SQUID Magnetometer at the "Unitat de Mesures Magnètiques (Universitat de Barcelona)". Five different magnetic fields were used for the DC susceptibility measurements, 3000 (2–300 K), 1000, 198, 44 and 13.5 G (2–30 K). AC susceptibility measurements were performed at two frequencies 10 and 997 Hz in the temperature range of 10–2.2 K and 10 and 900 Hz in the temperature range of 3.85–3.95 K, with an alternating field of 4 G. ZFC and FC measurements were performed at 85 G in the temperature range of 2–7 K. Pascal's constants were used to estimate the diamagnetic corrections for the compounds. The experimental data were fit by using the expansion series of Lines for an antiferromagnetic quadratic-layer of Mn(II) ions22 given by $Ng2\beta\ 2/\chi|J| = 3\Theta + (\Sigma Cn/\Theta n-1)$ in which $\Theta = kT/|J|S(S + 1)$, C1 = 4, C2 = 1.448, C3 = 0.228, C4 = 0.262, C5 = 0.119, C6 = 0.017, and N, g, and β have their usual meanings. This expression is based on the spin Hamiltonian $H = -\Sigma nnJSi \cdot Sj$, where Σnn runs over all pairs of the nearest-neighbor spins I and j. The fit of the susceptibility data was performed by minimising the function $R = \Sigma[(\chi MT)exp - (\chi MT)calc]2/\Sigma[(\chi MT)exp]2$.

Crystallographic data collection and refinement

A specimen of C16H18MnO6, with approximate dimensions of 0.100 mm × 0.100 mm × 0.200 mm, was used for the X-ray crystallographic analysis. The X-ray intensity data were collected on a D8 Venture system equipped with a multilayer monochromator and a Mo microfocus (λ = 0.71073 Å). The frames were integrated with the Bruker SAINT software package using a Bruker Saint algorithm. The integration of the data using a monoclinic unit cell yielded a total of 7101 reflections with the maximum θ angle of 24.71° (0.85 Å resolution), of which 1361 was independent (average redundancy 5.219, completeness = 99.8%, Rint = 5.98%, Rsig = 4.28%) and 1084 (79.65%) was greater than 2σ(F2). The final cell constants a = 16.057(2) Å, b = 6.8909(9) Å, c = 7.2259(10) Å, β = 94.608(5)°, and volume = 796.94(19) Å3, are based upon the refinement of the XYZ-centroids of reflections above 20σ(I). Data were corrected for absorption effects using the multi-scan method (SADABS).28 The calculated minimum and maximum transmission coefficients (based on crystal size) are 0.6068 and 0.7451.

The structure was solved and refined using the Bruker SHELXTL software package,29 using the space group P21/c, with Z = 2 for the formula unit, C16H18MnO6. The final anisotropic full-matrix least-squares refinement on F2 with 143 variables converged at R1 = 4.25%, for the observed data and wR2 = 11.30% for all data. The goodness-of-fit was 1.081. The largest peak in the final difference electron density synthesis was 0.546 e− Å−3 and the largest hole was −0.605 e− Å−3 with an RMS deviation of 0.080 e− Å−3. On the basis of the final model, the calculated density was 1.505 g cm−3 and F(000) was 374 e−.

Table S1 of the ESI† contains the crystallographic data collection and structure refinement details.

Computational details

The computational study of the electronic structure and magnetic properties of [Mn(3-MeC6H4COO)2(H2O)2] (1) has been performed using standard hybrid Density Functional Theory (DFT) based methods for periodic systems as implemented in the CRYSTAL09 program24 which has the advantage of using Gaussian atomic basis functions. A detailed description of the mathematical formulation and the algorithms in the CRYSTAL code has been previously published30–34 and is omitted here. Two different Gaussian atomic basis sets have been used to represent the electronic distributions in the system. In the first set of calculations, the TZVP35 standard all electron Gaussian basis set (or BS1) has been used for all the atoms to provide the best estimate for J1 and for the nature of the electronic structure of the material using the conventional crystallographic cell. However, to extract an estimate of the J2 and J3 values using large supercells we have to simplify the computational approach by using smaller basis sets (or BS2): for the Mn atoms a Hay and Wadt small core pseudopotential36 completed with a 311(d31)G basis set37 for external electrons, and for the nonmetallic atoms a 3-1G basis for H, a 6-31G for C and a 6-31d1G for O.38 A comparison of the results obtained from these two different computational approaches and the numerical estimates of the dominant J1 values shows that their values are consistent and provided confidence on the accuracy of

the smaller basis sets. In order to compute the band structure and the properties of the system the B3LYP39,40 and PBE041 (also known as PBE1PBE42) hybrid DFT functionals have been used. Very strict computational parameters have been adopted to ensure enough accuracy to calculate energy differences smaller than 10−6 Hartree (0.2 cm−1). Note that the energy differences between different magnetic solutions are of the order of 20–25 cm−1 thus providing enough precision to extract the values of the relevant magnetic coupling constants.

The calculations of the electronic band structure of this system, using the single and double cells depicted in Fig. 7 and 8, show that the open shell magnetic solutions are much more stable than the closed shell (or diamagnetic) solution. Analysis of the charge and spin densities of the different magnetic solutions, using Mulliken population analysis, shows that the spin density is strongly localized on the Mn(II) ions in all cases. The B3LYP calculations on the most stable AF solution assign a spin density of 4.86 unpaired electrons and a positive charge of 2.24 electrons for each Mn atom, in agreement with the expected values for the Mn2+ ions. The C, H and O centers show an important covalence as suggested by the corresponding overlap populations of the bonded atoms with a very small spin density on C and O of the carboxylate groups due to spin polarization (<±0.02 electrons). The density of states (DOS) for the AF ground state are shown in Fig. S6 of the ESI.† The PBE0 calculations provided very similar results.

Molecular electronic structure calculations on a cluster model have been performed for estimating J1. To this end, a molecular fragment was cut from the crystal including the two nearest-neighbour Mn2+ ions and its coordination sphere (outer ligands and a carboxylate bridge) with [Mn2(ROO)7(H2O)4]3− stoichiometry. The cluster model calculations have been performed using the Gaussian package43 and standard Gaussian all electron basis sets (6-3111+G for Mn and 6-31G* for H, C, and O). The spin unrestricted B3LYP and PBE0 functionals have been used to calculate the FM and AF solutions of this molecular fragment in the broken symmetry approach.23,25

CONCLUSIONS

The crystal structure of Mn(II) 3-methylbenzoate, [Mn(3-MeC6H4COO)2(H2O)2]n, shows a rhomboidal layer, where the adjacent Mn(II) ions are bridged through only one carboxylate group with a syn–anti conformation. The magnetic exchange between the neighbor ions is weakly antiferromagnetic ($J = -0.52$ cm^{-1}, $g = 2.04$), and at a low temperature the χMT curve shows a ferromagnetic order with TB = 3.8 K. The spatial disposition of the coordination polyhedra and their junction through only one carboxylate ligand with a syn–anti conformation is scarce and, to the best of our knowledge, there is only one reported system showing a low temperature magnetic order.16,17 Computational studies based on periodic electronic structure calculations describe this system as an antiferromagnetic insulator, with an indirect gap of 4.6 eV at the B3LYP level. Using the energies of the significant spin states on the magnetic cell and some higher supercells, the first-, secondand third-neighbour magnetic coupling constants have been estimated. The results show that a weak antiferromagnetic interaction between the adjacent Mn(II) ions dominates the magnetic structure with two very weak (two orders of magnitude lower) antiferromagnetic interactions between the nonadjacent Mn(II) ions, precluding the negligible effect of frustration caused by J2 and J3 interactions in the magnetic response of the system. The absence of the calculated positive magnetic coupling constants supports the fact that spin canting must be responsible for the ferromagnetic behavior experimentally observed at low temperatures due to the tilting of the Mn(II) coordination octahedra. The overall results provide a full

ACKNOWLEDGEMENTS

This research was supported by the Spanish MINECO, the Agencia Estatal de Investigación (AEI) and Fondo Europeo de Desarrollo Regional (FEDER) (projects CTQ2012-30662, CTQ2015-63614-P, CTQ2015-64618-R and CTQ2016-76423-P) and, in part, by Generalitat de Catalunya (grants 2017SGR13, 2017SGR348 and XRQTC).

REFERENCES

1 S. Durot, C. Policar, G. Pelosi, F. Bisceglie, T. Mallah and J. P. Mahyt, Inorg. Chem., 2003, 42, 8072–8080.

2 B. C. Dave and R. S. Czernuszewicz, Inorg. Chim. Acta, 1998, 281, 25–35.

3 M. Chen, M. Hu, H. Zhao, J.-Y. Tian and C.-S. Liu, Z. Anorg. Allg. Chem., 2016, 642, 778–784.

4 J. Cui, Z. Lu, Y. Li, Z. Guo and H. Zheng, Cryst. Growth Des., 2012, 12, 1022–1031.

5 Q. B. Bo, H. Y. Wang, D. Q. Wang, Z. W. Zhang, J. L. Miao and G. X. Sun, Inorg. Chem., 2011, 50, 10163–10177.

6 M. Chen, Z. W. Wang, E. C. Sañudo, H. Zhao and C. Sen Liu, Inorg. Chem. Commun., 2014, 4 3, 121–125.

7 Y. He, Z. Guo, S. Xiang, Z. Zhang, W. Zhou, F. R. Fronczek, S. Parkin, S. T. Hyde, M. O'Keeffe and B. Chen, Inorg. Chem., 2013, 52, 11580–11584.

8 L.-P. Zhang, J.-F. Ma, J. Yang, Y.-Y. Pang and J.-C. Ma, Inorg. Chem., 2010, 49, 1535–1550.

9 Y. L. Wu, F. S. Guo, G. P. Yang, L. Wang, J. C. Jin, X. Zhou, W. Y. Zhang and Y. Y. Wang, Inorg. Chem., 2016, 55, 6592–6596.

10 L. L. Qu, Y. L. Zhu, Y. Z. Li, H. Bin Du and X. Z. You, Cryst. Growth Des., 2011, 11, 2444–2452.

11 W. Li, Z.-F. Ju, Q.-X. Yao and J. Zhang, CrystEngComm, 2008, 10, 1325–1327.

12 D. Čechová, A. Martišková, Z. Padělková, L. Gal'a, L. Dlháň, D. Valigura, M. Valko, R. Boča and J. Moncol, Polyhedron, 2014, 79, 129–137.

13 G. Zhuang, L. Tan, W. Chen, J. Zheng, H. Yao, X. Zhong and J. Wang, Inorg. Chem. Front., 2014, 1, 526–533.

14 J.-H. Wang, G.-M. Tang, Y.-T. Wang, T.-X. Qin and S. W. Ng, CrystEngComm, 2014, 16, 2660–2683.

15 M. Dan and C. N. R. Rao, Chemistry, 2005, 11, 7102–7109.

16 R. Sibille, A. Mesbah, T. Mazet, B. Malaman, S. Capelli and M. François, J. Solid State Chem., 2012, 186, 134–141.

17 J. A. Kaduk, Acta Crystallogr., Sect. B: Struct. Sci., 2002, 58, 815–822.

18 D.-F. Weng, Z.-M. Wang and S. Gao, Chem. Soc. Rev., 2011, 40, 3157–3181.

19 P. Kar, P. M. Guha, M. G. B. Drew, T. Ishida and A. Ghosh, Eur. J. Inorg. Chem., 2011, 2011, 2075–2085.

20 S.-D. Han, J.-P. Zhao, Y.-Q. Chen, S.-J. Liu, X.-H. Miao, T.-L. Hu and X.-H. Bu, Cryst. Growth Des., 2014, 14, 2–5.

21 L. Cheng, W. X. Zhang, B. H. Ye, J. Bin Lin and X. M. Chen, Eur. J. Inorg. Chem., 2007, 2, 2668–2676.

22 M. E. Lines, J. Phys. Chem. Solids, 1970, 31, 101–116.

23 P. Rivero, I. de P. R. Moreira and F. Illas, J. Phys.: Conf. Ser., 2008, 117, 12025.

24 R. Dovesi, V. R. Saunders, C. Roetti, R. Orlando, C. M. Zicovich-Wilson, F. Pascale, B. Civalleri, K. Doll, N. M. Harrison, I. Bush, Ph. D'Arco and M. Llunell, CRYSTAL2009, 2010.

25 I. de P. R. Moreira and F. Illas, Phys. Chem. Chem. Phys., 2006, 8, 1645–1659.

26 F. Palacio, M. Andrés, R. Horne and A. J. van Duyneveldt, J. Magn. Magn. Mater., 1986, 54–57, 1487–1488.

27 G. Deacon, Coord. Chem. Rev., 1980, 33, 227–250.

28 Sheldrick, SADABS, Version 2008/1, Bruker AXS Inc., 2008.

29 G. Sheldrick, XT Program for the Solution of Crystal Structures, Bruker AXS Inc., Madison, WI.

30 C. Pisani, R. Dovesi and C. Roetti, Hartree–Fock ab initio treatment of crystalline systems, Springer Verlag, Heidelberg, 1988, vol. 48.

31 C. Pisani, Lecture Notes in Chemistry, in Quantum- Mechanical Ab-Initio Calculation of the Properties of Crystalline Materials, ed. C. Pisani, Springer-Verlag, Berlin, 1996, ch. 3, vol. 67, pp. 47–75.

32 R. Dovesi, R. Orlando, C. Roetti, C. Pisani and V. R. Saunders, Phys. Status Solidi B, 2000, 217, 63–88.

33 M. D. Towler, A. Zupan and M. Causa, Comput. Phys. Commun., 1996, 98, 181–205.

34 R. Dovesi, C. Roetti, C. Freyria-Fava, M. Prencipe and V. R. Saunders, Chem. Phys., 1991, 156, 11–19.

35 M. F. Peintinger, D. V. Oliveira and T. Bredow, J. Comput. Chem., 2013, 34, 451–459.

36 P. J. Hay and W. R. Wadt, J. Chem. Phys., 1985, 82, 270–310.

37 R. A. Evarestov, E. A. Kotomin, E. Heifets, J. Maier and G. Borstel, Solid State Commun., 2003, 127, 367–371.

38 C. Gatti, V. R. Saunders and C. Roetti, J. Chem. Phys., 1994, 101, 10686–10696.

39 A. D. Becke, J. Chem. Phys., 1993, 98, 5648–5652.

40 C. Lee, W. Yang and R. G. Parr, Phys. Rev. B: Condens. Matter Mater. Phys., 1988, 37, 785–789.

41 C. Adamo and V. Barone, J. Chem. Phys., 1999, 110, 6158–6170.

42 M. Ernzerhof and G. E. Scuseria, J. Chem. Phys., 1999, 110, 5029–5036.

43 M. J. Frisch, G. W. Trucks, H. B. Schlegel, G. E. Scuseria, M. A. Robb, J. R. Cheeseman, G. Scalmani, V. Barone, G. A. Petersson, H. Nakatsuji, X. Li, M. Caricato, A. Marenich, J. Bloino, B. G. Janesko, R. Gomperts, B. Mennucci, H. P. Hratchian, J. V. Ortiz, A. F. Izmaylov, J. L. Sonnenberg, D. Williams-Young, F. Ding, F. Lipparini, F. Egidi, J. Goings, B. Peng, A. Petrone, T. Henderson, D. Ranasinghe, V. G. Zakrzewski, J. Gao, N. Rega, G. Zheng, W. Liang, M. Hada, M. Ehara, K. Toyota, R. Fukuda, J. Hasegawa, M. Ishida, T. Nakajima, Y. Honda, O. Kitao, H. Nakai, T. Vreven, K. Throssell, J. A. Montgomery, Jr., J. E. Peralta, F. Ogliaro, M. Bearpark, J. J. Heyd, E. Brothers, K. N. Kudin, V. N. Staroverov, T. Keith, R. Kobayashi, J. Normand, K. Raghavachari, A. Rendell, J. C. Burant, S. S. Iyengar, J. Tomasi, M. Cossi, J. M. Millam, M. Klene, C. Adamo, R. Cammi, J. W. Ochterski, R. L. Martin, K. Morokuma, O. Farkas, J. B. Foresman and D. J. Fox, Gaussian 09, Revisions D.01, Gaussian Inc., Wallingford CT, 2013. Paper Dalton Transactions 3724

Legends to figures

Figure. 1. View of a layer in the crystal structure of 1.

Figure. 2. Rhombic fragment of a layer in the crystal structure of 1, showing the syn–anti conformation of the carboxylate ligands. The 3-MeC6H4 groups of the bridging ligands are omitted for clarity. Note that all manganese centers are crystallographically equivalent.

Figure. 3. View of a sheet (the 3-MeC6H4 groups are omitted for clarity) where the arrows show the elongation axes on the coordination octahedral of Mn(II) ions. Note that the blue arrows represent the axes of the same length and the different visual size is due to the perspective.

Figure. 4 χMT vs. T and χM vs. T (inset) plots for compound 1, at two magnetic fields (3000 and 200 G); solid line corresponds to the best fit in the 300–5 K range (data referred to one Mn(II) ion).

Figure. 5. ffect of the magnetic field on the χMT vs. T and χM vs. T (inset) plots at low temperatures.

Figure. 6. Thermal dependence of the zero-field cooled (ZFC) and fieldcooled (FC) χMT curves under an applied field of 85 G.

Figure. 7. Field dependency of the magnetization of 1 at 2 K, and first derivative, dM/dH, is shown in the inset.

Figure. 8. Representation of the relevant magnetic coupling constants J1, J2 and J3 represented in the FM solution using the conventional crystallographic cell. Black circles represent Mn ions with alpha (up) spin density.

Figure 9. Representation of the spin distributions of the ferromagnetic (FM) and antiferromagnetic (AF) solutions. Black (white) circles represent Mn ions with alpha (beta) spin density.

Figure. 10. Representation of the spin distributions of the relevant magnetic solutions based on two different supercells as discussed in the text. Black (white) circles represent Mn ions with alpha (beta) spin density.

Figure. 11 Energy scheme and coupling constant mapping for the relevant magnetic states described in the text.

FIGURE 1

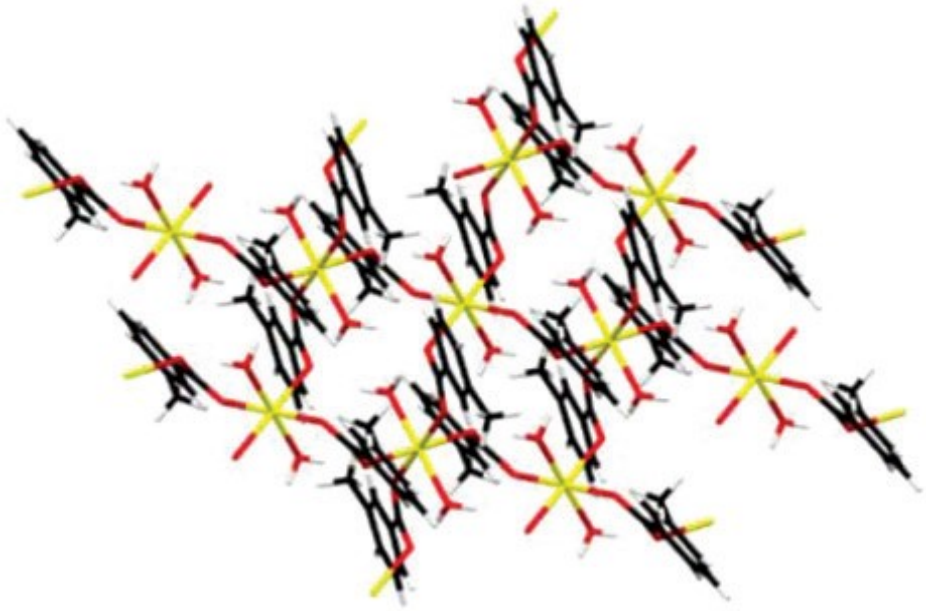

493 **FIGURE 2**

494

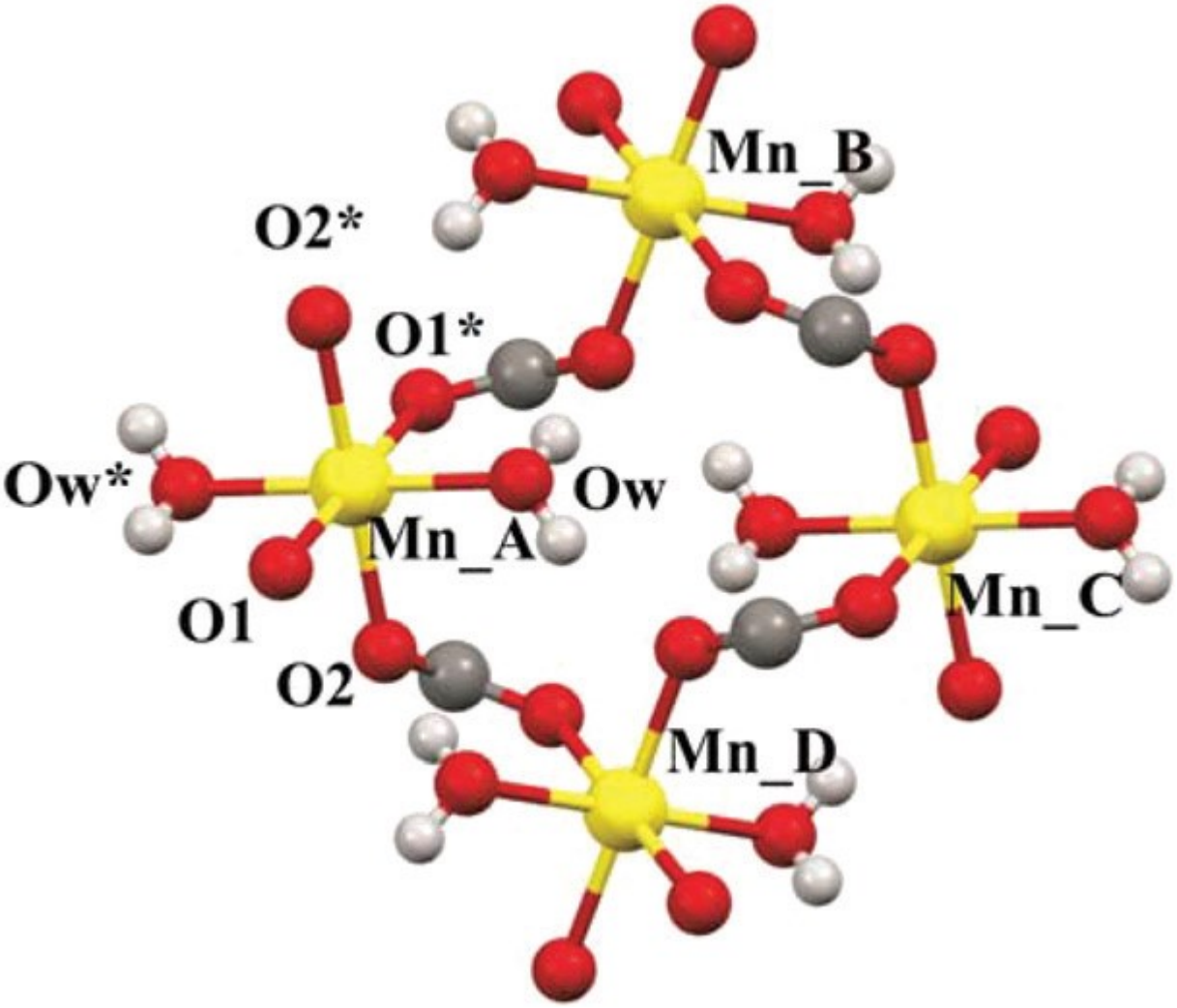

495

496

FIGURE 3

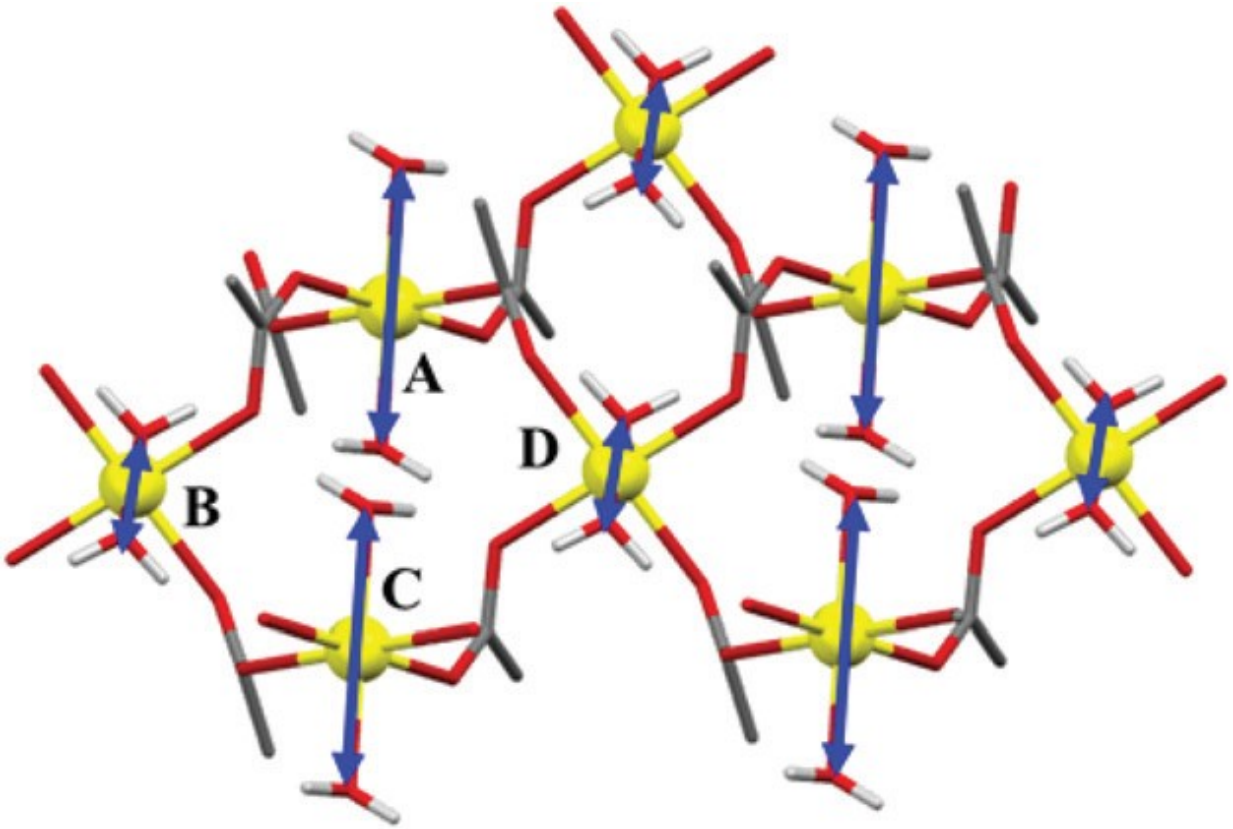

FIGURE 4

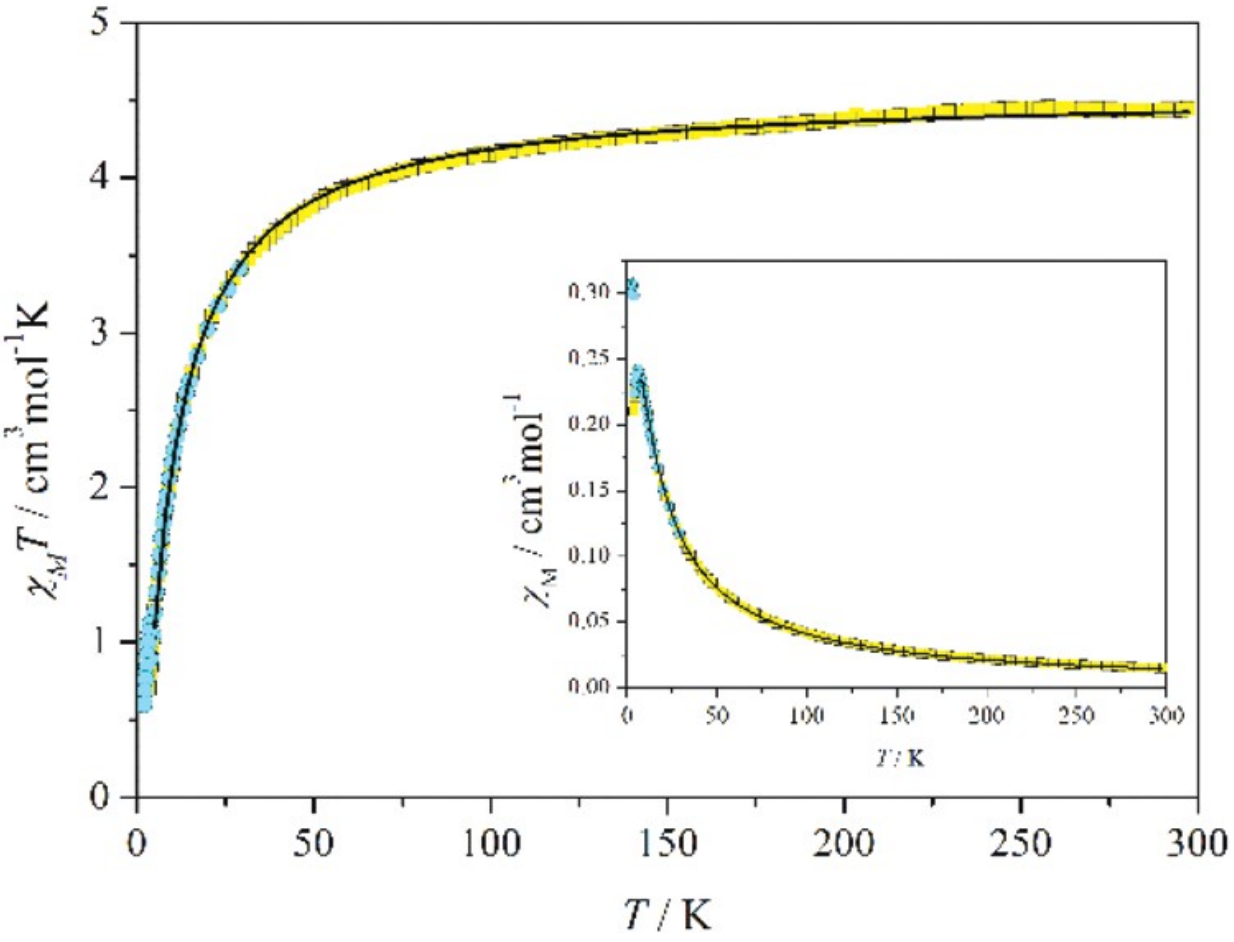

507 **FIGURE 5**

508

509

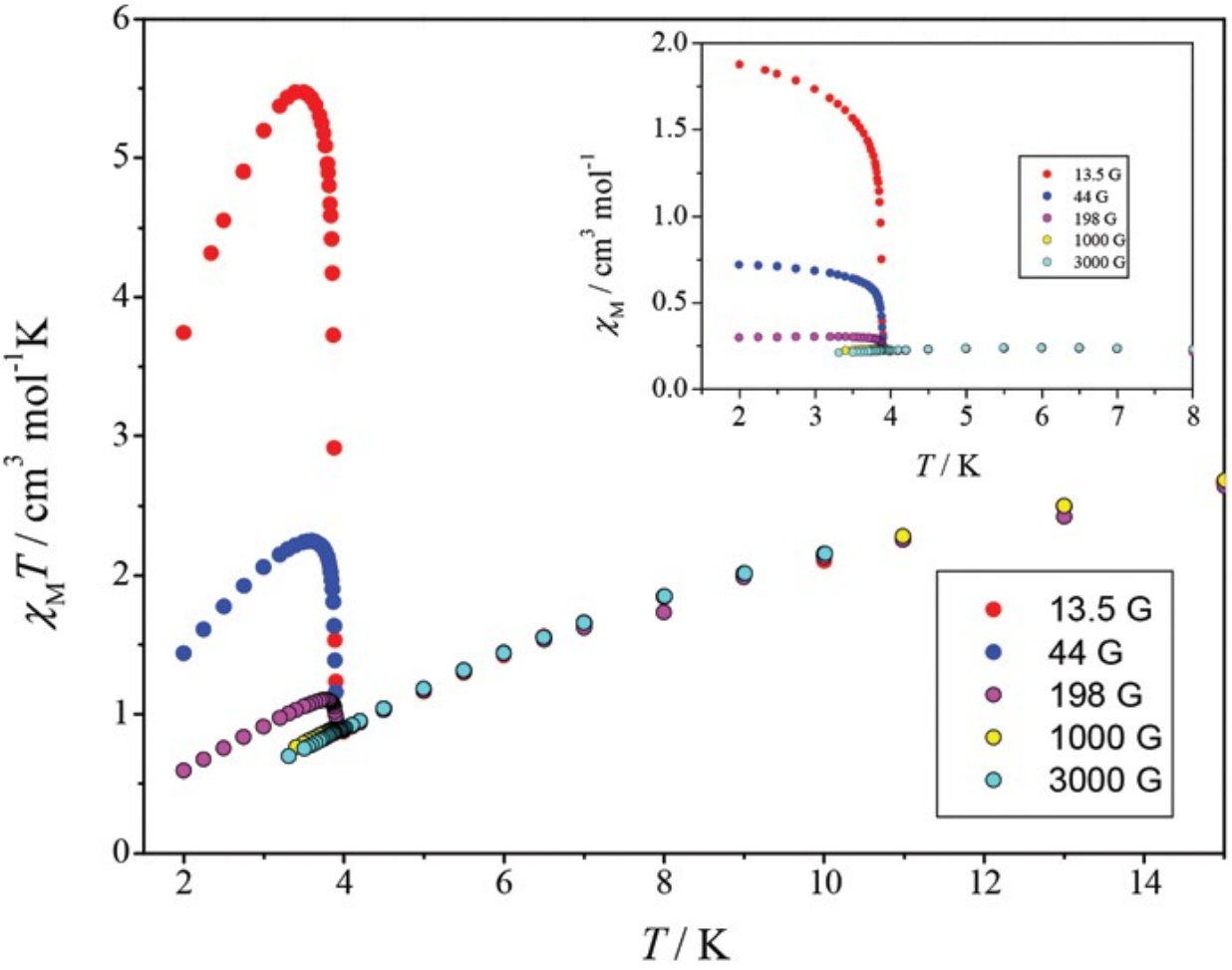

510

511

FIGURE 6

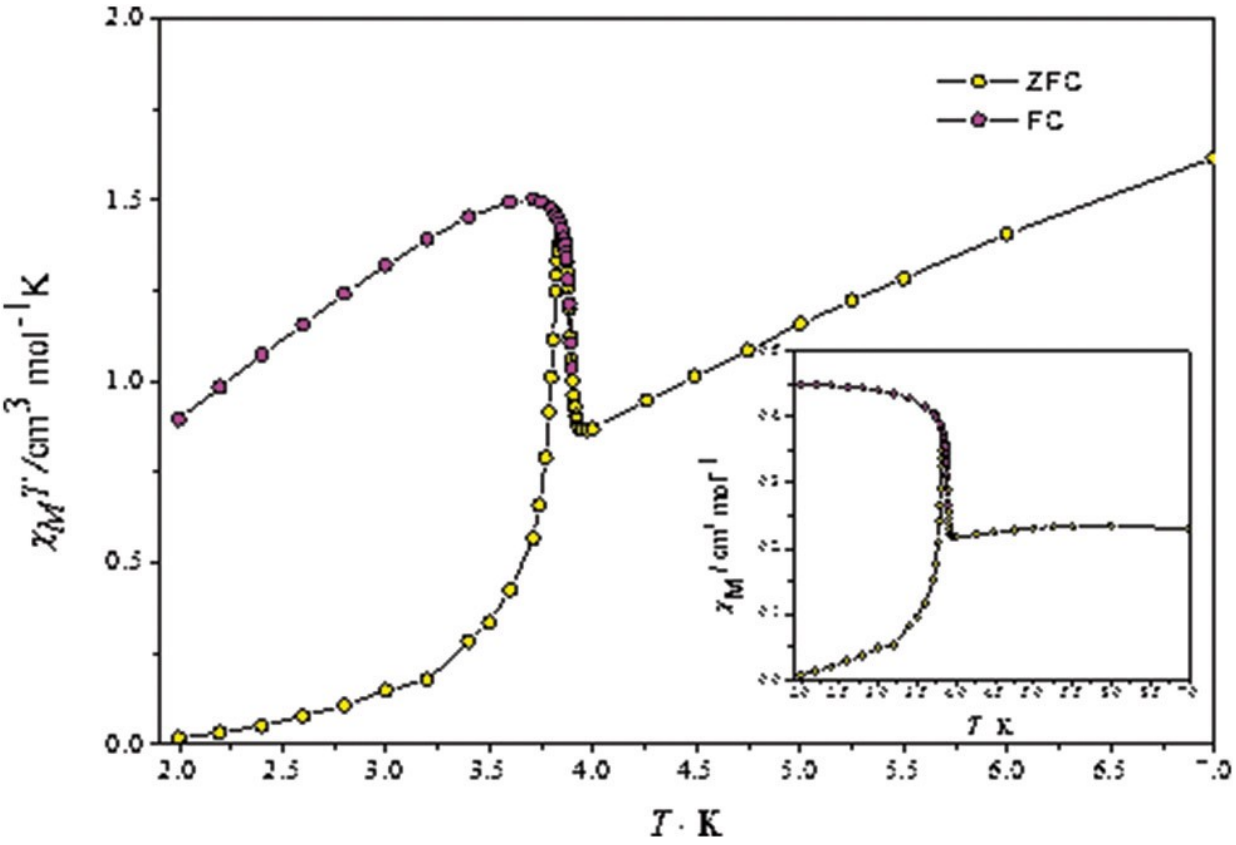

FIGURE 7

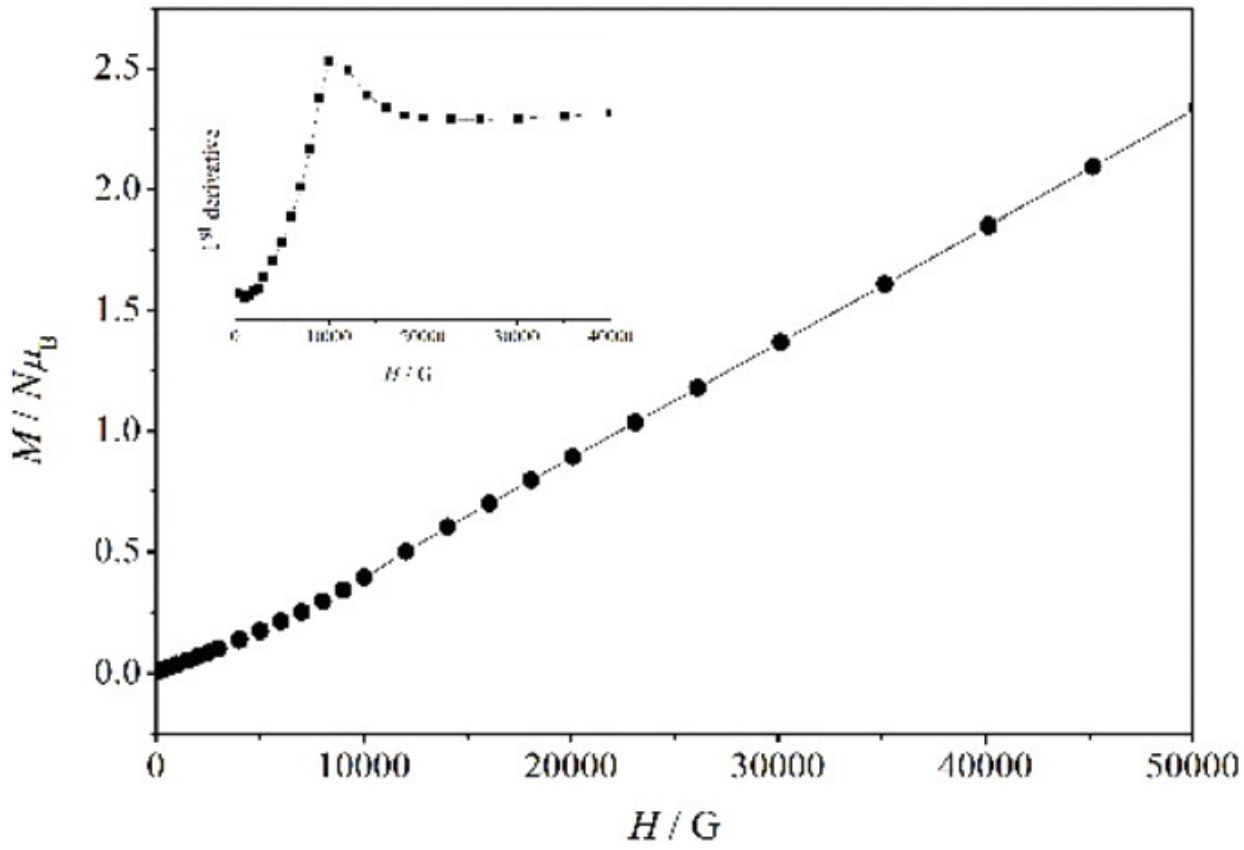
2.5
2.0
1.5
1.0
0.5
0.0
$M / N\mu_B$
0
10000
20000
30000
40000
50000
H / G
1st derivative
H / G

521 **FIGURE 8**

522

523

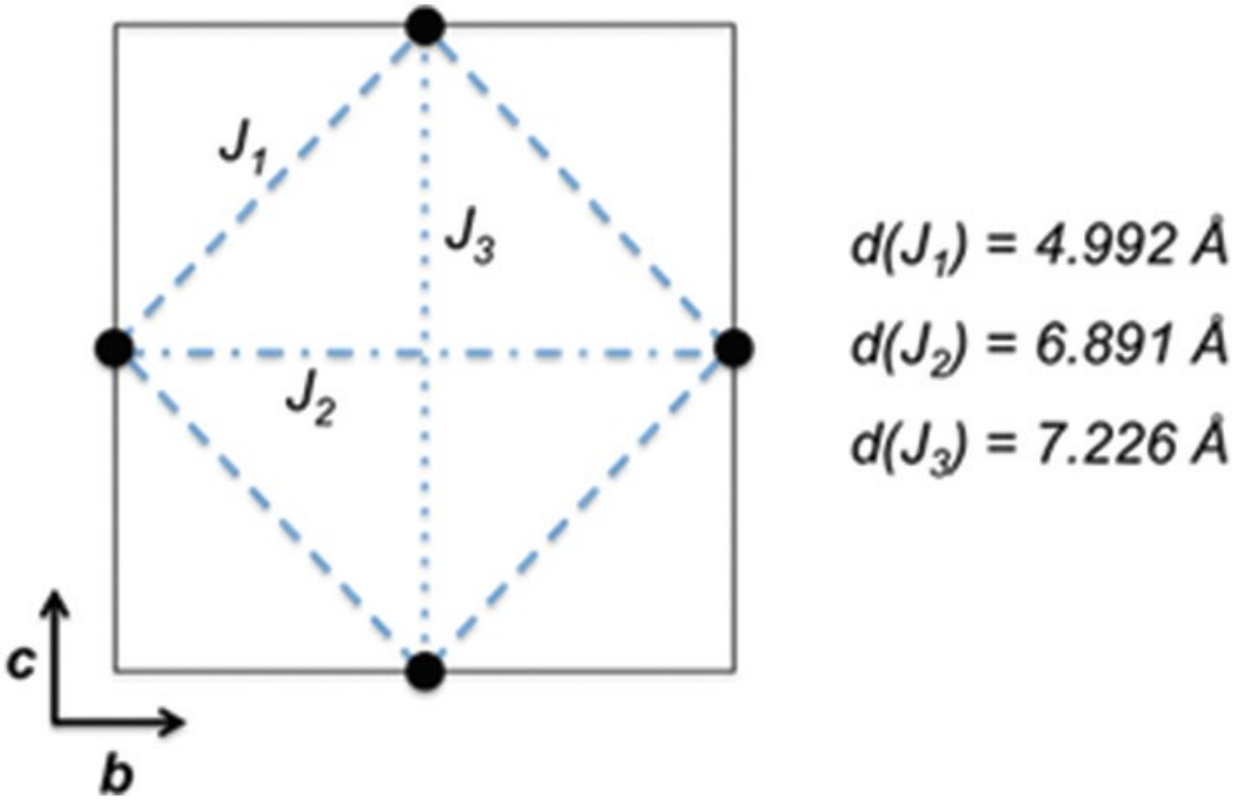

524

525

FIGURE 9

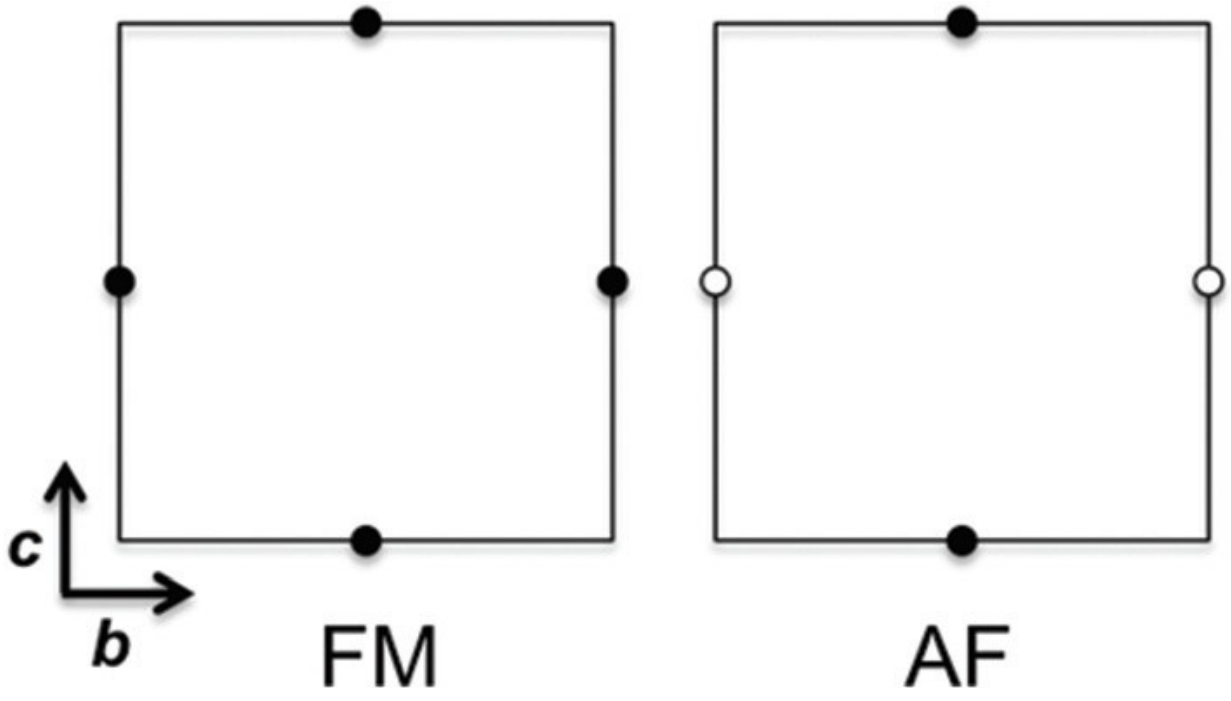

FIGURE 10

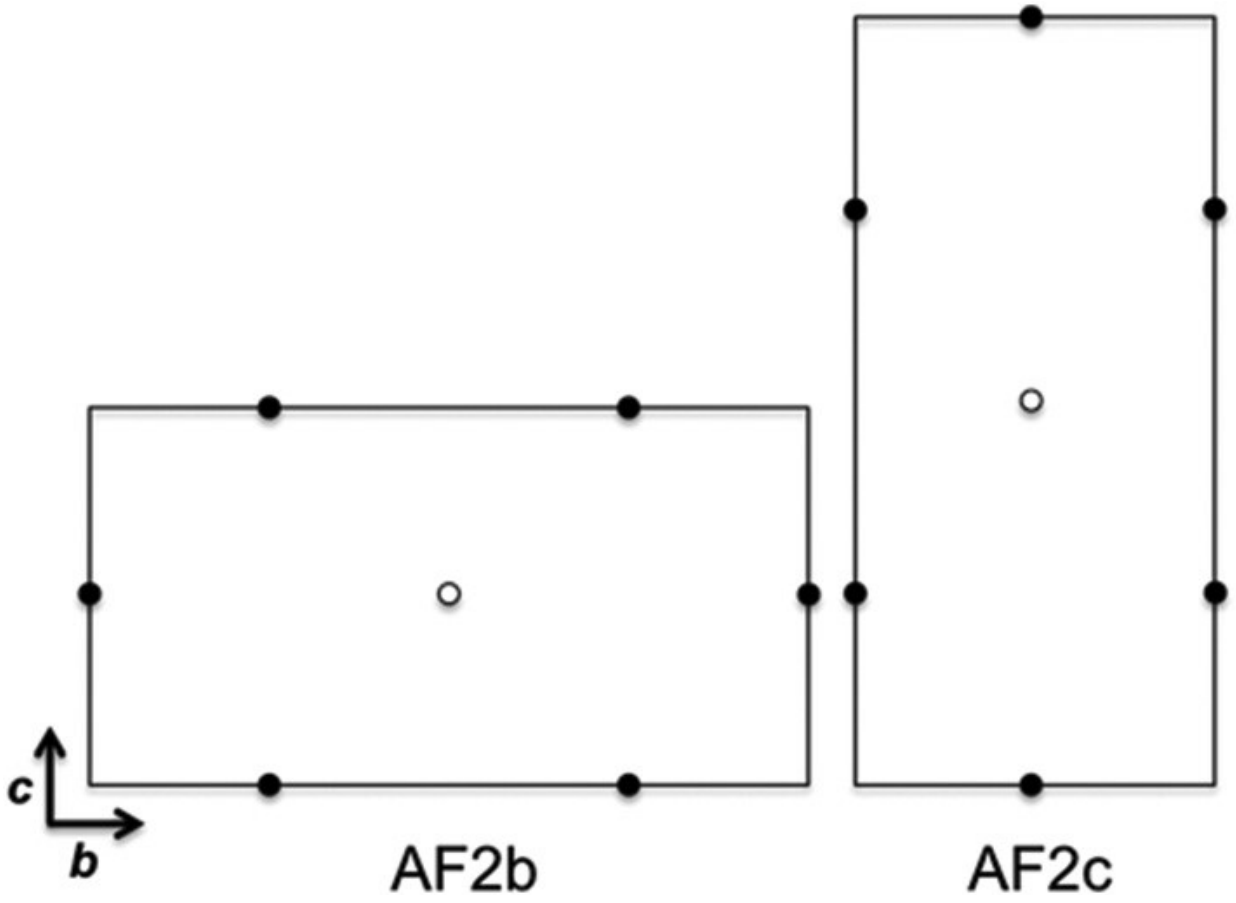

FIGURE 11

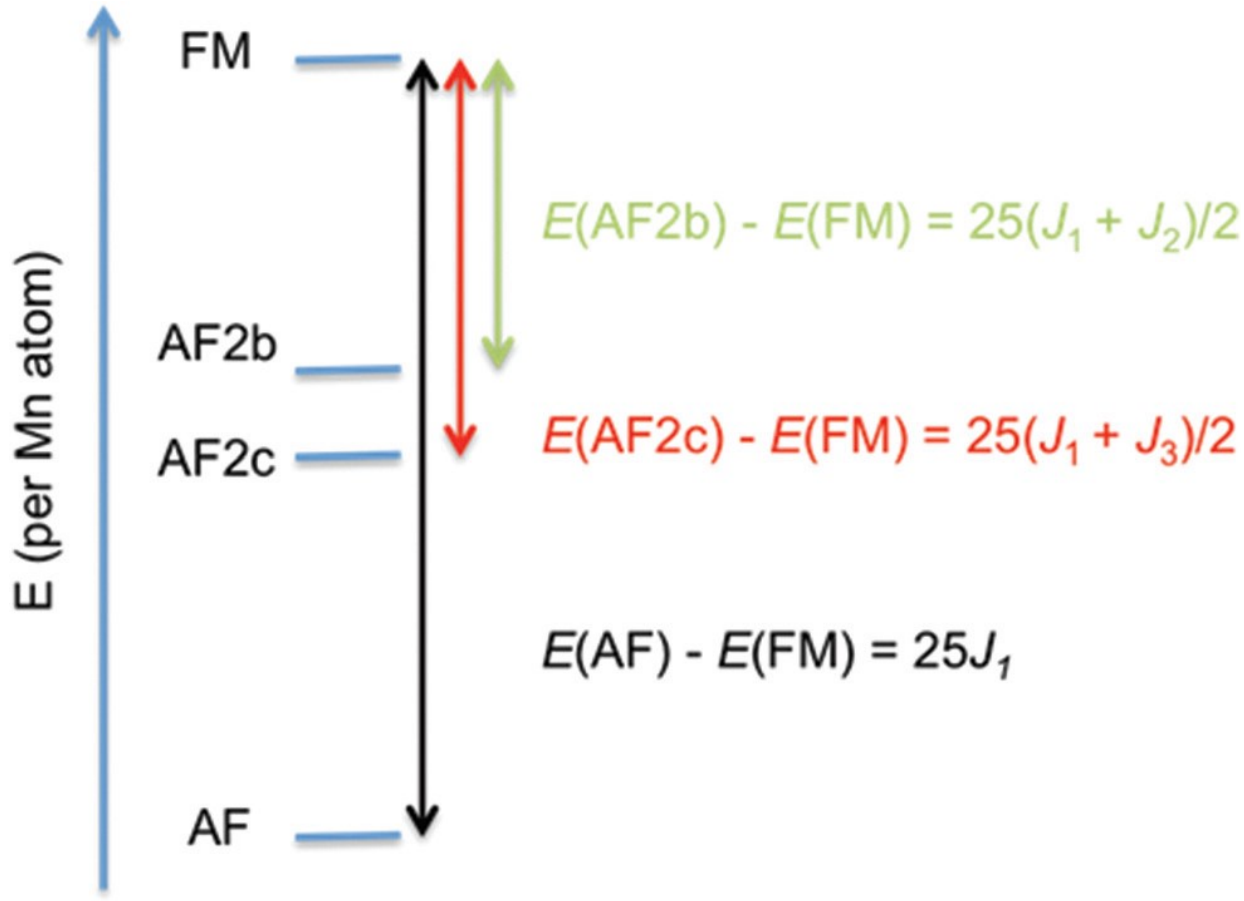
FM
AF2b
AF2c
AF
E (per Mn atom)
E(AF2b) - E(FM) = 25(J1 + J2)/2
E(AF2c) - E(FM) = 25(J1 + J3)/2
E(AF) - E(FM) = 25J1

541 **Table 1**.. Selected bond lengths (Å) and angles (°) for compound 1

542

Mn–O1	2.172(2)	O1–Mn–OW*	88.14(9)
Mn–O1*	2.172(2)	O1*–Mn–OW	88.14(9)
Mn–OW	2.178(2)	O1*–Mn–OW*	91.86(9)
Mn–OW*	2.178(2)	O1–Mn–OW	91.86(9)
Mn–O2	2.175(2)	O1–Mn–O2	88.47(9)
Mn–O2*	2.175(2)	O1*–Mn–O2*	88.47(9)
Mn_A···Mn_B	4.992	O1–Mn–O2*	91.53(9)
Mn_A···Mn_C	6.891	O1*–Mn–O2	91.53(9)
Mn_B···Mn_D	7.226	OW–Mn–O2*	88.77(8)
O1–Mn–O1*	180.00	OW*–Mn–O2	88.77(8)
OW–Mn–OW*	180.00	OW*–Mn–O2*	91.23(8)
O2–Mn–O2*	180.00	OW–Mn–O2	91.23(8)
O1–C1_C2_C3	6.8(5)	Mn–O1–C1	133.03
O2–C1–C2–C7	6.0(5)	Mn–O2–C1	127.78

543